



Epigenetics Hot Paper

How to cite: *Angew. Chem. Int. Ed.* **2021**, *60*, 8760–8765

International Edition: doi.org/10.1002/anie.202017200

German Edition: doi.org/10.1002/ange.202017200

Structure-Guided Discovery of a Potent and Selective Cell-Active Inhibitor of SETDB1 Tudor Domain

Yinping Guo⁺, Xin Mao⁺, Liang Xiong⁺, Anjie Xia, Jing You, Guifeng Lin, Chengyong Wu, Luyi Huang, Yiwei Wang, and Shengyong Yang*

Abstract: *SET domain bifurcated protein 1 (SETDB1) is a histone lysine methyltransferase that promotes the silencing of some tumour suppressor genes and is overexpressed in many cancers. SETDB1 contains a unique tandem tudor domain (TTD) that recognizes histone H3 sequences containing both methylated and acetylated lysines. Beginning with the identification of a hit compound (Cpd1), we discovered the first potent and selective small molecule SETDB1-TTD inhibitor (R,R)-59 through stepwise structure-guided optimization. (R,R)-59 showed a K_D value of $0.088 \pm 0.045 \mu\text{M}$ in the ITC assay. The high potency of (R,R)-59 was well explained by the cocrystal structure of the (R,R)-59-TTD complex. (R,R)-59 is an endogenous binder competitive inhibitor. Evidence has also demonstrated its cellular target engagement. Interestingly, the enantiomer (S,S)-59 did not show activity in all the assays, highlighting the potential of (R,R)-59 as a tool compound in exploring the biological functions of SETDB1-TTD.*

Histone “reader” proteins, which use structurally conserved domains to recognize and engage histone post-translational modifications (PTMs), play a critical role in the functional interpretation of the so-called “histone code” and hence in regulating gene expression and signal transduction.^[1] The dysregulation of histone reader proteins has been linked to the development of various human diseases, particularly cancer.^[2] As a consequence, the histone reader proteins have become promising targets for drug development.^[3] Currently, many histone reader proteins have been identified.^[4] Among them, tudor domains, a type of methyllysine reader proteins, have recently attracted attention due to their association with various cancers.^[5] Nevertheless, unlike the widely studied bromodomain (BRD)-containing proteins (acetyllysine readers), which have a large amount of inhibitors reported with several having already reached clinical trials,^[6] a very limited number of small molecule inhibitors targeting tudor domain-containing proteins have been reported.^[7] And only two potent and selective inhibitors were disclosed, namely

MS31^[7b] and VinSpinln,^[7c] both of which are inhibitors of the Tudor domain containing protein, Spindlin1.

Human SETDB1 is a histone lysine methyltransferase that specifically trimethylates histone H3 lysine 9 (H3K9me3). It has been demonstrated to be an oncogene and found to be overexpressed in many cancers.^[8] SETDB1 is a multidomain protein containing unique tandem tudor domains (TTD), a methyl-DNA binding domain (MBD), and a classical catalytic SET domain.^[9] Tudor domains often recognize methylated lysine.^[10] A very recent study by Jurkowska et al demonstrated that TTD in SETDB1 (SETDB1-TTD) specifically binds to histone H3 tails containing K9 methylation combined with K14 acetylation (H3K9me/K14ac).^[11] However, the exact biological function of SETDB1-TTD remains unclear. Small molecule inhibitors that selectively disrupt the binding of SETDB1-TTD to its endogenous binders could be useful tool compounds for revealing the biological function of SETDB1-TTD and could also be potential disease intervention agents. Recently, Mader et al reported a fragment hit for SETDB1-TTD with a weak binding affinity (K_D : 5 mM).^[12] Nevertheless, no potent and selective small molecule tool compounds targeting SETDB1-TTD have been reported at present. The work herein describes the discovery of such a tool compound.

To identify SETDB1-TTD inhibitors, a screening was performed against an in-house chemical library, which contains about 5000 compounds synthesized by our group, by using a differential scanning fluorimetry (DSF) assay with 10 μM TTD protein and 100 μM test compounds. One compound, 3,5-dimethyl-2-[(3*R*,5*R*)-1-methyl-5-phenylpiperidin-3-yl]amino}-3,5-dihydro-4*H*-pyrrolo[3,2-*d*]pyrimidin-4-one (Cpd1, Figure 1A), showed a thermal shift (ΔT_m) of 1.58 °C in the DSF assay. The thermal shift values were also dose dependent (Figure S1). The bioactivity of this compound was further validated by an isothermal titration calorimetry (ITC) assay, which gave a K_D value of $4.4 \pm 1.7 \mu\text{M}$ (Figure 1B).

Further structural optimization of Cpd1 was then carried out. To this end, we first solved the X-ray crystal structure of TTD in complex with Cpd1. As shown in Figure 1C and Figure 1D (PDB entry: 7C9N), Cpd1 binds to the region between tudor 2 and tudor 3, which is different from the Spindlin1 inhibitors MS31 and VinSpinln; they bind to tudor 2 (MS31) or the region between tudor 1 and tudor 2 (VinSpinln) of Spindlin1 (Figure S2). The 1-methyl-3-phenylpiperidine moiety resides in an aromatic cage formed by Y301, Y268, W275, Y277 and F297. The nitrogen (-NH) linking pyrrolo[3,2-*d*]pyrimidin-4-one and piperidine ring forms a hydrogen bond with the phenol-oxygen of Y268. The

[*] Y. Guo,^[†] X. Mao,^[†] L. Xiong,^[†] A. Xia, J. You, G. Lin, C. Wu, L. Huang, Y. Wang, Prof. Dr. S. Yang
State Key Laboratory of Biotherapy and Cancer Center, West China Hospital, Sichuan University
Chengdu, Sichuan 610041 (P. R. China)
E-mail: yangsy@scu.edu.cn

[†] These authors contributed equally to this work.

Supporting information and the ORCID identification number(s) for the author(s) of this article can be found under:
 <https://doi.org/10.1002/anie.202017200>.

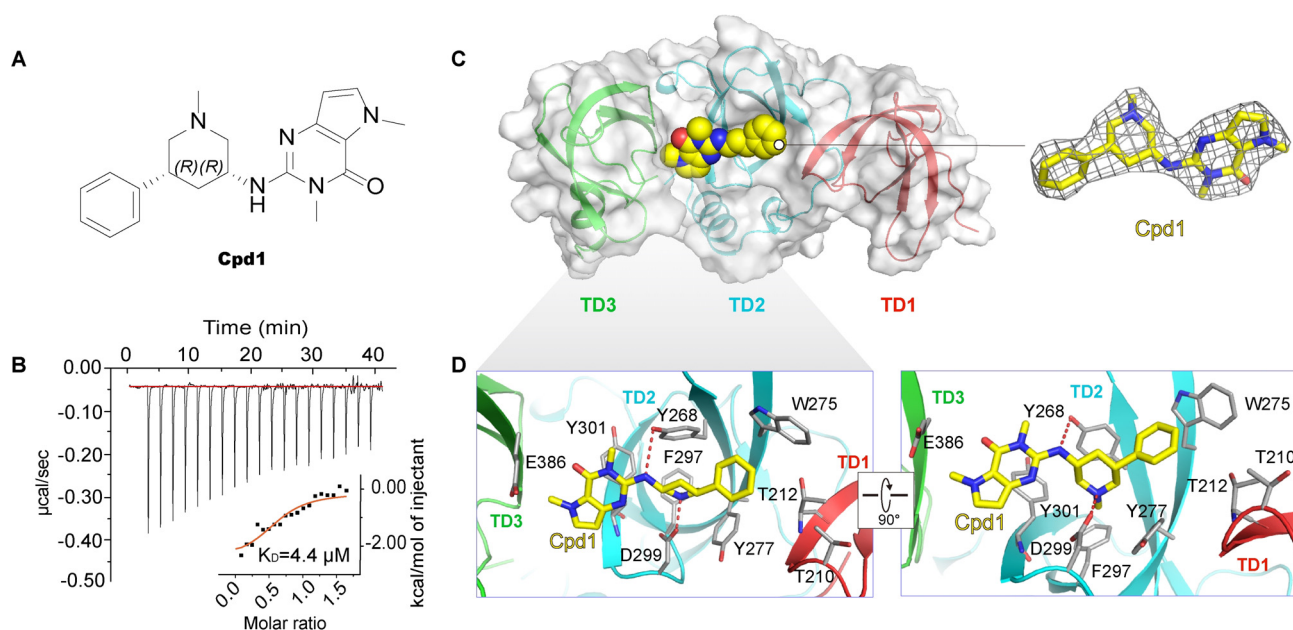


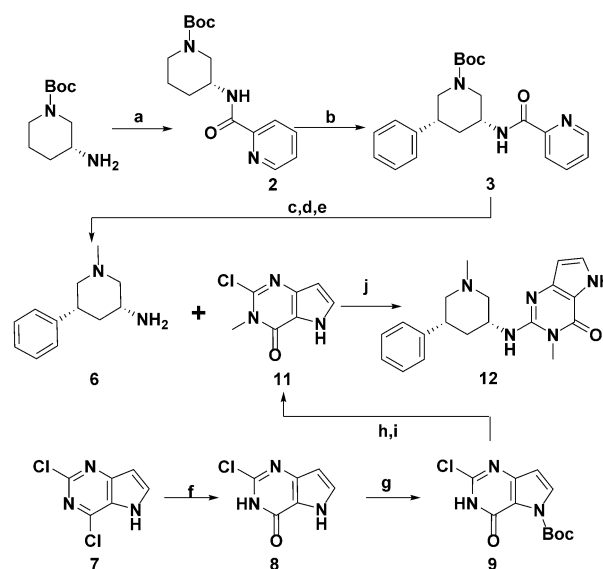
Figure 1. Bioactivity of **Cpd1** and the crystal structure of the **Cpd1**-TTD complex (PDB entry 7C9N). A) The chemical structure of **Cpd1**. B) ITC analysis of **Cpd1** ($K_D = 4.4 \pm 1.7 \mu\text{M}$). C) Surface view of the complex of TTD (surface and cartoon representation) and **Cpd1** (thick yellow stick representation) (left) and the electron density of **Cpd1** (yellow stick representation) (right). D) The interaction mode of **Cpd1** (yellow stick representation) with TTD.

ionized nitrogen in 1-methylpiperidine forms an electrostatic interaction with D299.

According to the cocrystal structure, we assumed that three sites of **Cpd1** could be modified to improve its binding affinity. The first site is the methyl group on the pyrrole nitrogen because replacing the 5-position methyl group with hydrogen could enhance the binding affinity due to a new hydrogen bonding interaction between pyrrole nitrogen (-NH) and E386. The second group is the phenyl group because there seems to be some incompletely occupied space in its surroundings. The third group is the 3-methyl group of pyrrolo[3,2-*d*]pyrimidin-4-one since there is a large empty space around the methyl group.

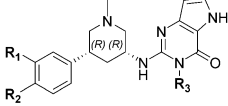
Accordingly, in the first step, we replaced the 5-position methyl group on the pyrrole nitrogen with hydrogen and synthesized a new compound (**12**) (Figure S3A). Scheme 1 shows the synthetic route of compound **12**. Commercially available (*R*)-1-Boc-3-aminopiperidine reacted with the bidentate directing group picolinic acid to produce intermediate **2**, which underwent C(sp³)-H arylation with iodobenzene to afford enantiomerically pure **3**. This intermediate was further converted to key intermediate **6** through Boc deprotection (**4**), reductive amination (**5**), and cleavage of the bidentate directing group. Commercially available 2,4-dichloro-pyrrolo[3,2-*d*]pyrimidine (**7**) underwent a series of reactions, including hydrolysis (**8**), Boc protection (**9**), nucleophilic substitution (**10**) and Boc deprotection, to generate another key intermediate **11**. Finally, **11** underwent a SNAr reaction with **6** to produce target compound **12**.

DSF and ITC assays were adopted to test the bioactivity of compound **12**. This compound indeed showed significantly improved potency compared with **Cpd1**; the ΔT_m and K_D values of compound **12** are 5.16 °C and $1.6 \pm 0.22 \mu\text{M}$, respectively (Table 1, Figure S3B). We then solved the crystal



Scheme 1. Synthesis of compound **12**. Reagents and conditions: a) picolinic acid, HATU, DIEA, DCM, rt, 24 h, 85%; b) aryl iodides, Pd(OAc)₂, Ag₂CO₃, 2,6-dimethylbenzoic acid, *t*-BuOH, 120 °C, 36 h, 66%, >99% *ee*; c) TFA, DCM, rt, 4 h; d) 37% formaldehyde, NaBH-(OAc)₃, AcOH, DCM, rt, 6 h, 88%; e) NaOH, *i*-PrOH, 85 °C, 18 h, 80%; f) 1 M NaOH (aq), 100 °C, 16 h, 92%; g) Boc₂O, TEA, DMAP, DMF, rt, overnight, 82%; h) iodomethane, NaH, anhydrous DMF, 40 °C, overnight; i) TFA, DCM, rt, 4 h, 46% over two steps; j) DIPEA, NMP, 150 °C, 2 h, 14%.

structure of TTD in complex with compound **12**. The crystal structure (PDB entry: 7CAJ) shows that compound **12** occupies the same binding site of TTD with the same pose as **Cpd1**, and key interactions between **Cpd1** and TTD remain (Figure S3C). Replacement of the 5-position methyl with

Table 1: Bioactivities of the newly synthesized compounds.


Cpd	R ₁	R ₂	R ₃	Δ <i>T</i> _m [°C] ^[a]	K _D [μM]
12	H	H	Me	5.16	1.6 ± 0.22
41	H	MeO	Me	3.26	0.72 ± 0.12
42	H	CF ₃ O	Me	1.89	2.0 ± 1.4
43	Br	H	Me	4.40	0.54 ± 0.05
44	H	PhO	Me	4.03	0.52 ± 0.51
45	H	BnO	Me	8.15	0.21 ± 0.13
46	BnO	H	Me	2.33	1.9 ± 0.25
47	H	<i>n</i> Bu	Me	2.79	0.91 ± 0.18
48	H	OH	Me	3.79	1.5 ± 0.13
56	H	BnO	<i>i</i> Pr	3.87	0.47 ± 0.12
57	H	BnO	Et	6.71	0.26 ± 0.10
58	H	BnO	Pr	6.04	0.36 ± 0.004
(<i>R,R</i>)-59	H	BnO	Allyl	5.79	0.088 ± 0.045
60	H	BnO	Bn	NA ^[b]	NB ^[c]
(<i>S,S</i>)-59	H	BnO	Allyl	NA	NB

[a] Protein concentration 10 μM, compound concentration 100 μM;

[b] NA: no activity; [c] NB: no binding.

hydrogen shortens the distance between E386 and the 5-position -NH (from 4 Å to 2.6 Å), enabling the formation of a hydrogen bond between them, as expected.

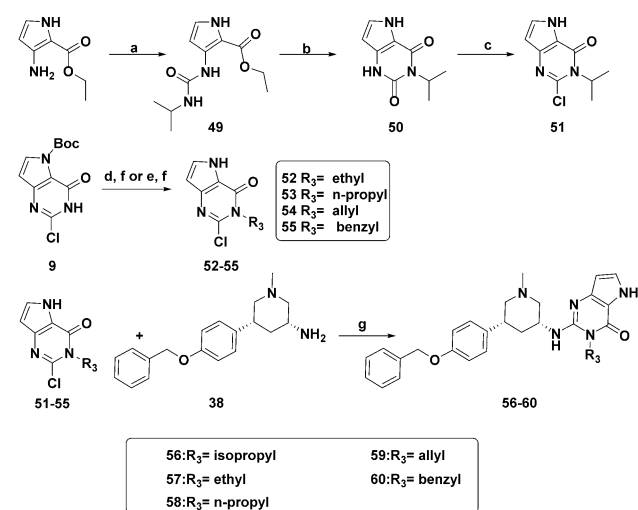
We then optimized the phenyl group, which resides in a hydrophobic pocket formed by residues T210, T212, and W275 in tudor 1 and tudor 2. Various substituents were installed on the phenyl ring, which generated eight new compounds (**41–48**). Compounds **41–47** were synthesized following a similar route to that for compound **12** (Scheme S5). Compound **48** was prepared by the Pd/C catalysed debenylation of compound **45**.

The bioactivities of the synthesized compounds are shown in Table 1. Unexpectedly, all the newly synthesized compounds with either small or bulky substituents showed reduced or at most comparable activity with respect to the unsubstituted compound **12**. The only exception is compound **45** (Figure S3D), which bears a *para*-benzyloxy group. This compound showed elevated potency with Δ*T*_m and K_D values of 8.15°C and 0.21 ± 0.13 μM, respectively (Table 1, Figure S3E). To understand the intrinsic reason, we solved the crystal structure of TTD in complex with compound **45**. As shown in Figure S3F, compound **45** resides in the same binding site with the same pose as **Cpd1** and **12**. Notably, the indole ring of W275 undergoes a 23° counter clockwise rotation, which positions the indole ring parallel to the benzene ring of benzyloxy, forming an F-type π-π stack interaction (Figure S3G). Obviously, *para*-methoxyl (**41**), *para*-trifluoromethoxy (**42**), *meta*-bromine (**43**), *para*-phenoxy (**44**), *para*-*n*-butyl (**47**), and *para*-hydroxyl (**48**) could not form such interactions due to either the lack of a benzene ring (**41–43**, **47**, **48**) or insufficient length (**44**). Although *meta*-benzyloxy derivative **46** harbours a benzyloxy group like **45**, the *meta*-position benzyloxy cannot induce a rotation of the indole ring of W275 to form π-π interactions and instead causes unfavourable steric interactions.

We finally modified the 3-methyl group of pyrrolo[3,2-*d*]pyrimidin-4-one. Various alkyl groups were used to replace the methyl group, and five new compounds (**56–60**) were synthesized. Scheme 2 shows the reaction routes for these compounds. Commercially available 3-amino-2-ethoxycarbonylpyrrole reacted with 2-isocyanatopropane to produce **49**, which then underwent a cyclization reaction and successive chlorination to generate intermediate **51**. Nucleophilic substitution reactions of **9** with bromoethane, 1-bromopropane, allyl bromide and benzyl bromide gave corresponding intermediates **52–55**. Compounds **51–55** were then reacted with the previously obtained intermediate **38** to generate the final products **56–60**.

The bioactivities of compounds **56–60** are shown in Table 1. Compounds **56–58** and **60** bearing isopropyl, ethyl, *n*-propyl, and benzyl at the 3-position of pyrrolo[3,2-*d*]pyrimidin-4-one, respectively, exhibited a decreased binding affinity compared with **45**, indicating that a bulkier substituent is not preferred. However, **59** with a propenyl group displayed improved potency with a K_D value of 0.088 ± 0.045 μM in the ITC assay (Table 1, Figure 2A, and B). It also dose-dependently stabilized the TTD protein in the DSF assay (Figure 2C).

To explain this unusual phenomenon, we again solved the crystal structure of TTD in complex with **59** (Figure 2D). Compound **59** also resides in the same binding site with the same pose as **Cpd1**, **12** and **45**. All the key interactions between compound **45** and TTD are maintained. We noticed that the phenolic hydroxyl of Y268 faces the C=C double bond of propenyl with C-O distances of 2.995 Å (C1-O) and 2.822 Å (C2-O), implying that a σ*-π interaction formed (Figure 2E). This could explain why **59** has a higher potency than the others.



Scheme 2. Synthesis of compounds **56–60**. Reagents and conditions: a) 2-isocyanatopropane, Et₃N, toluene, rt, 24 h, 95%; b) 1 M KOH (MeOH), reflux, 2 h, 60%; c) POCl₃, 100°C, 24 h, 23%; d) haloalkanes, NaH, anhydrous DMF, 50°C, overnight; e) benzyl bromide, NaH, LiBr, DME/DMF, 65°C, 8 h; f) TFA, DCM, rt; 34–78%, over two steps; g) DIPEA, NMP, 150°C, 2 h, 12–24%.

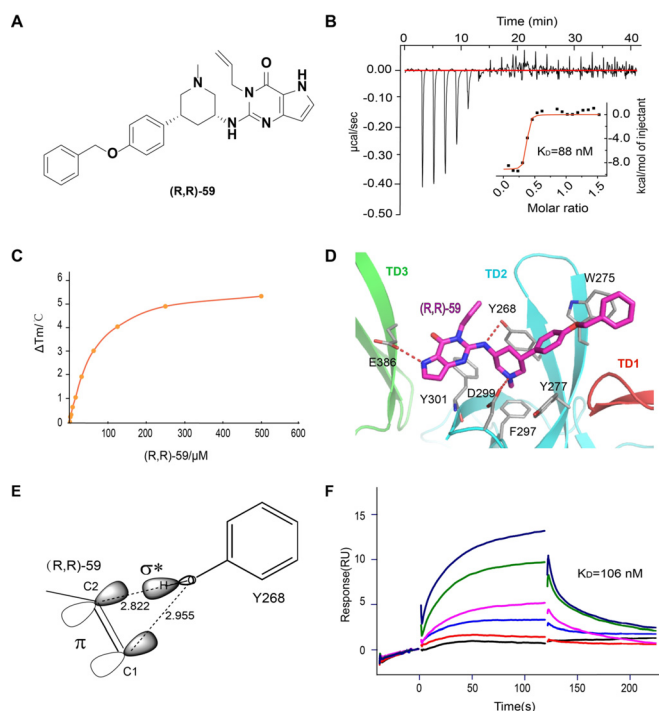


Figure 2. Biophysical activities and the binding mode of **(R,R)-59**. A) The chemical structure of **(R,R)-59**. B) ITC analysis of **(R,R)-59** ($K_D = 0.088 \pm 0.045 \mu\text{M}$). C) Dose-dependent curve of **(R,R)-59** in the DSF assay. D) Binding modes of **(R,R)-59** with SETDB1-TTD (PDB entry: 7CJT). E) Presumed $\sigma^*-\pi$ interaction between the phenolic hydroxyl of Y268 and the C=C double bond of propenyl in **(R,R)-59**. F) SPR analysis of **(R,R)-59**.

Because **59** is a chiral compound with an *(R,R)* conformation, the other enantiomer *(S,S)-59* was also synthesized (for clarity, **59** will be denoted as *(R,R)-59* below). The synthetic route of *(S,S)-59* is very similar to that of *(R,R)-59*; the only difference is that the starting material (*S*)-3-amino-1-*N*-*boc*-piperidine was used instead of (*R*)-3-amino-1-*N*-*boc*-piperidine in the synthesis of *(S,S)-59* (Scheme S6, Figure S3H). Interestingly, this compound did not show activity in either the DSF or ITC assay (Table 1, Figure S3I).

To further validate the bioactivity of *(R,R)-59*, a surface plasmon resonance (SPR) assay, which is another commonly used biophysical activity assay method, was performed. In this assay, *(R,R)-59* showed a K_D value of $0.106 \pm 0.002 \mu\text{M}$ against TTD (Figure 2F). Again, the enantiomer *(S,S)-59* did not exhibit activity in this assay.

To examine the selectivity of *(R,R)-59*, we expressed and purified 16 other tudor domains from different tudor domain-containing proteins. The ITC assay was adopted to test the bioactivity of *(R,R)-59* against these proteins (Figure 3A, Table S2). *(R,R)-59* did not show activity against 14 of the 16 tested tudor domains ($K_D > 100 \mu\text{M}$). 53BP1 and JMJD2A were the only two tudor domain proteins for which *(R,R)-59* showed some activity; the K_D values were $4.3 \mu\text{M}$ and $86 \mu\text{M}$, respectively. Furthermore, *(R,R)-59* was tested against 32 BRD proteins using the DSF assay. Among the 32 proteins, it showed no activity or very weak activity (Table S3, Figure S4A). All these results indicate that *(R,R)-59* has considerable selectivity for SETDB1-TTD.

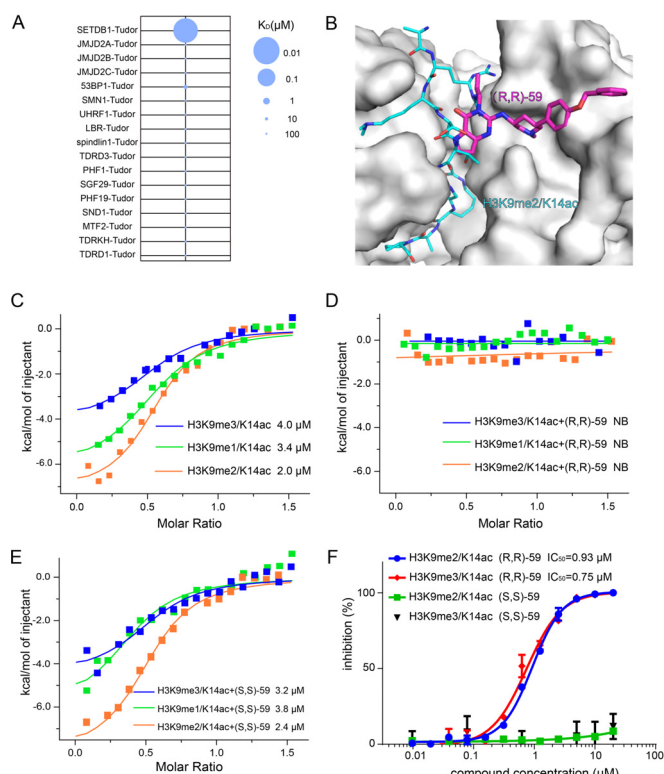


Figure 3. Selectivity and competition assays of **(R,R)-59**. A) Binding affinity of **(R,R)-59** with 17 tudor domain-containing proteins measured by ITC. B) A superposition of crystal structures of the TTD-**(R,R)-59** complex (PDB entry: 7CJT) and TTD-H3 peptide (PDB ID: 6BHD). C) ITC analysis of different H3 peptides (H3K9me3/K14ac, H3K9me2/K14ac, H3K9me1/K14ac) and SETDB1-TTD. D) Competition experiment with **(R,R)-59** and different H3 peptides using ITC analysis. SETDB1-TTD protein was pretreated with **(R,R)-59** for 20 minutes and then titrated with different H3 peptides. E) Competition experiment with **(S,S)-59** and different H3 peptides using ITC analysis. SETDB1-TTD protein was pretreated with **(S,S)-59** for 20 minutes and then titrated with different H3 peptides. F) The HTRF test system consists of GST-SETDB1-TTD and biotinylated H3 peptides (Bio-H3K9me2/K14ac, and Bio-H3K9me3/K14ac), which is used to test the inhibitory activity of compounds against the TTD-endogenous H3 peptide interaction.

SETDB1-TTD has been demonstrated to bind to doubly modified histone H3 with the combination of K9 methylation and K14 acetylation (H3K9me/K14ac). Further crystal structures revealed that the H3 peptides bind to the groove between TD2 and TD3.^[11] A superposition of the crystal structures of the TTD-**(R,R)-59** complex (PDB entry: 7CJT) and TTD-H3 peptide (PDB ID: 6BHD) shows an overlap between the **(R,R)-59** and H3 peptide binding sites (Figure 3B), implying that **(R,R)-59** could prevent or at least interfere with the binding of H3 peptide. To verify this point, we performed ITC experiments with differently modified H3(4–19) peptides and TTD. The dissociation constants (K_D) of TTD and H3K9me/K14ac, H3K9me2/K14ac, and H3K9me3/K14ac were $3.36 \mu\text{M}$, $1.96 \mu\text{M}$, and $3.98 \mu\text{M}$, respectively (Figure 3C), which are comparable to the literature values.^[11] After incubating TTD with **(R,R)-59** for 20 minutes, the binding of H3 peptides with TTD could not be detected (Figure 3D), suggesting that **(R,R)-59** completely

prevented the association of H3 peptides and TTD. In the same assay, the enantiomer (**S,S**)-**59** did not show an impact on the association of H3 peptides and TTD (Figure 3E). Further, a homogenous time-resolved fluorescence (HTRF) assay was used to test the inhibitory activity of (**R,R**)-**59** against the TTD—H3 peptide interaction. The measured IC_{50} values of (**R,R**)-**59** against the TTD—H3K9me2/K14ac and TTD—H3K9me3/K14ac interactions were 0.93 μ M and 0.75 μ M, respectively (Figure 3F). Again, the enantiomer (**S,S**)-**59** did not exhibit obvious activity in this assay. All the results suggest that (**R,R**)-**59** is an endogenous binder competitive inhibitor.

To verify whether (**R,R**)-**59** interacts with SETDB1-TTD in intact cells, we performed a cellular thermal shift assay (CETSA); CETSA is a method based on the thermal stabilization of target proteins upon drug binding. In this assay, HEK293T cells stably transfected with a pLVX-mCherry-N1-SETDB1-TTD plasmid were used (Figure S4B). The cells were treated with (**R,R**)-**59** and (**S,S**)-**59** in different concentrations at 50 °C and lysed by repeated freeze-thaw cycles with liquid nitrogen. The protein content of the soluble fraction in the lysate was determined by western blot analysis. The results showed that (**R,R**)-**59** at concentrations of ≥ 5 μ M could efficiently and dose-dependently stabilize the SETDB1-TTD protein in HEK293T cells. In contrast, the enantiomer (**S,S**)-**59** did not exhibit a stabilizing effect in all the tested concentrations (Figure 4A, and B). To further examine the activity of (**R,R**)-**59** in living cells, we performed a fluorescence recovery after photobleaching (FRAP) assay

using EGFP tagged SETDB1-TTD (wild-type) and Y268A mutant plasmids; the Y268A mutation has been demonstrated to lead a specific loss in the binding of H3 endogenous binders.^[11] Cells were treated with (**R,R**)-**59** (6 μ M), (**S,S**)-**59** (6 μ M), or DMSO for 18 hours. The normalized half-life recovery times ($t_{1/2}$) of (**S,S**)-**59** and DMSO treatment groups were 1.50 ± 0.31 s and 1.45 ± 0.34 s, respectively. Both the (**R,R**)-**59** treatment group and Y268A mutant group showed a significantly decreased $t_{1/2}$ (1.05 ± 0.33 s, and 1.01 ± 0.17 s, respectively) (Figure 4C), meaning that the majority of the protein is mobile. All the experimental results clearly indicate (**R,R**)-**59**'s cellular target engagement.

Finally a RNA-sequencing (RNA-seq) experiment was conducted to explore the effect of (**R,R**)-**59** on global gene expression. In this experiment, human acute monocytic leukemia THP-1 cells were treated with (**R,R**)-**59** (10 μ M), (**S,S**)-**59** (10 μ M), or DMSO for 24 hours, and the cells were then collected for RNA-seq analysis. (**R,R**)-**59** treatment significantly affected the expression of 72 genes (> 4 -fold). Among them, 49 genes were uniquely affected by (**R,R**)-**59**, which may be attributed to the effect of SETDB1-TTD (Figure 4D). Even so, the biological significance of (**R,R**)-**59** causing gene up-regulation or down-regulation still needs to be further studied.

In conclusion, we report the discovery of a potent and selective cell-active SETDB1-TTD inhibitor (**R,R**)-**59**. (**R,R**)-**59** and its inactive enantiomer (**S,S**)-**59** could serve as a pair of early-stage tool compounds for investigating biological functions and disease associations of SETDB1-TTD. Moreover, the current study together with recent discoveries of potent and selective small molecule inhibitors of Spindlin1^[7b,c] clearly demonstrated the feasibility of targeting tudor domains.

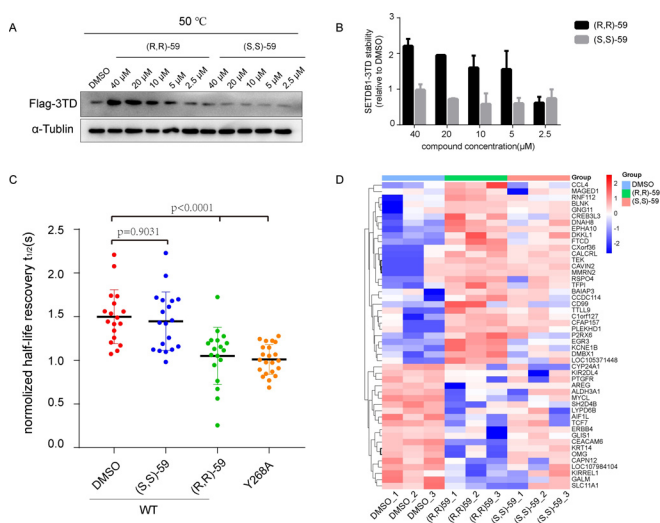


Figure 4. Cellular target engagement assays. A) The CETSA assay was carried out with Flag-SETDB1-TTD transfected HEK293T cells grown in the presence or absence of (**R,R**)-**59**/**(S,S)**-**59** for 6 h. B) Stabilization effect of Flag-SETDB1-TTD induced by (**R,R**)-**59** or (**S,S**)-**59** normalized to DMSO. C) The FRAP experiments using 293T cells transfected with EGFP-tagged SETDB1-TTD wild-type (WT) and Y268A mutant. The SETDB1-TTD group was treated with 6 μ M (**R,R**)-**59** or (**S,S**)-**59** (18 h). Eighteen cells were imaged for each group and one-way ANOVA with Dunnett's correction for multiple comparisons was used to detect significant differences ($P < 0.05$). D) Heat map of selected genes showing different regulation by (**R,R**)-**59**, (**S,S**)-**59**, or DMSO (up- or down- regulation > 4 -fold and $p < 0.05$ of (**R,R**)-**59**).

Acknowledgements

This work was supported by the National Natural Science Foundation of China (Grant No: 81930125, 21772130 and 81773633), and partly by the fast-track research fund of Sichuan Province (2020YFS0006) and 1.3.5 project for disciplines of excellence, West China Hospital, Sichuan University (ZYG18001). The authors thank the staffs from BL17U1, BL18U, and BL19U1 beamlines of National Facility for Protein Science Shanghai (NFPS) at Shanghai Synchrotron Radiation Facility (SSRF) for assistance during data collection. The ITC experiments were carried out at the Core Facilities at College of Life Sciences of Sichuan University.

Conflict of interest

The authors declare no conflict of interest.

Keywords: epigenetics · SETDB1 · structure-based optimization · tool compound · tudor domain

- [1] a) B. D. Strahl, C. D. Allis, *Nature* **2000**, *403*, 41–45; b) C. A. Musselman, M. E. Lalonde, J. Cote, T. G. Kutateladze, *Nat. Struct. Mol. Biol.* **2012**, *19*, 1218–1227.
- [2] a) M. A. Dawson, *Science* **2017**, *355*, 1147–1152; b) F. P. Vendetti, C. M. Rudin, *Expert Opin. Biol. Ther.* **2013**, *13*, 1273–1285.
- [3] a) P. Filippakopoulos, S. Knapp, *Nat. Rev. Drug Discovery* **2014**, *13*, 337–356; b) M. A. Dawson, T. Kouzarides, B. J. Huntly, *N. Engl. J. Med.* **2012**, *367*, 647–657.
- [4] a) N. Zaware, M. M. Zhou, *Curr. Opin. Chem. Biol.* **2017**, *39*, 116–125; b) C. H. Arrowsmith, M. Schapira, *Nat. Struct. Mol. Biol.* **2019**, *26*, 863–869.
- [5] a) R. Lu, G. G. Wang, *Trends Biochem. Sci.* **2013**, *38*, 546–555; b) Z. Ren, J. H. Ahn, H. Liu, Y. H. Tsai, N. V. Bhanu, B. Koss, D. F. Allison, A. Ma, A. J. Storey, P. Wang, S. G. Mackintosh, R. D. Edmondson, R. W. J. Groen, A. C. Martens, B. A. Garcia, A. J. Tackett, J. Jin, L. Cai, D. Zheng, G. G. Wang, *Blood* **2019**, *134*, 1176–1189.
- [6] a) Y. Duan, Y. Guan, W. Qin, X. Zhai, B. Yu, H. Liu, *MedChemComm* **2018**, *9*, 1779–1802; b) G. S. Sheppard, L. Wang, S. D. Fidanze, L. A. Hasvold, D. Liu, J. K. Pratt, C. H. Park, K. Longenecker, W. Qiu, M. Torrent, P. J. Kovar, M. Bui, E. Faivre, X. Huang, X. Lin, D. Wilcox, L. Zhang, Y. Shen, D. H. Albert, T. J. Magoc, G. Rajaraman, W. M. Kati, K. F. McDaniel, *J. Med. Chem.* **2020**, *63*, 5585–5623; c) A. G. Cochran, A. R. Conery, R. J. Sims 3rd, *Nat. Rev. Drug Discovery* **2019**, *18*, 609–628.
- [7] a) N. Bae, M. Viviano, X. Su, J. Lv, D. Cheng, C. Sagum, S. Castellano, X. Bai, C. Johnson, M. I. Khalil, J. Shen, K. Chen, H. Li, G. Sbardella, M. T. Bedford, *Nat. Chem. Biol.* **2017**, *13*, 750–756; b) Y. Xiong, H. Greschik, C. Johansson, L. Seifert, J. Bacher, K. S. Park, N. Babault, M. Martini, V. Fagan, F. Li, I. Chau, T. Christott, D. Dilworth, D. Barsyte-Lovejoy, M. Vedadi, C. H. Arrowsmith, P. Brennan, O. Fedorov, M. Jung, G. Farnie, J. Liu, U. Oppermann, R. Schule, J. Jin, *J. Med. Chem.* **2019**, *62*, 8996–9007; c) V. Fagan, C. Johansson, C. Gileadi, O. Monteiro, J. E. Dunford, R. Nibhani, M. Philpott, J. Malzahn, G. Wells, R. Faram, A. P. Cribbs, N. Halidi, F. Li, I. Chau, H. Greschik, S. Velupillai, A. Allali-Hassani, J. Bennett, T. Christott, C. Giroud, A. M. Lewis, K. V. M. Huber, N. Athanasou, C. Bountra, M. Jung, R. Schule, M. Vedadi, C. Arrowsmith, Y. Xiong, J. Jin, O. Fedorov, G. Farnie, P. E. Brennan, U. Oppermann, *J. Med. Chem.* **2019**, *62*, 9008–9025; d) G. Senisterra, H. Y. Zhu, X. Luo, H. Zhang, G. Xun, C. Lu, W. Xiao, T. Hajian, P. Loppnau, I. Chau, F. Li, A. Allali-Hassani, P. Atadja, C. Oyang, E. Li, P. J. Brown, C. H. Arrowsmith, K. Zhao, Z. Yu, M. Vedadi, *SLAS Discovery* **2018**, *23*, 930–940; e) M. T. Perfetti, B. M. Baughman, B. M. Dickson, Y. Mu, G. Cui, P. Mader, A. Dong, J. L. Norris, S. B. Rothbart, B. D. Strahl, P. J. Brown, W. P. Janzen, C. H. Arrowsmith, G. Mer, K. M. McBride, L. I. James, S. V. Frye, *ACS Chem. Biol.* **2015**, *10*, 1072–1081.
- [8] a) E. Orouji, A. Federico, L. Larribere, D. Novak, D. B. Lipka, Y. Assenov, S. Sachindra, L. Huser, K. Granados, C. Gebhardt, C. Plass, V. Umansky, J. Utikal, *Int. J. Cancer* **2019**, *145*, 3462–3477; b) Q. Fei, K. Shang, J. Zhang, S. Chuai, D. Kong, T. Zhou, S. Fu, Y. Liang, C. Li, Z. Chen, Y. Zhao, Z. Yu, Z. Huang, M. Hu, H. Ying, Z. Chen, Y. Zhang, F. Xing, J. Zhu, H. Xu, K. Zhao, C. Lu, P. Atadja, Z. X. Xiao, E. Li, J. Shou, *Nat. Commun.* **2015**, *6*, 8651.
- [9] Y. K. Kang, *Curr. Issues Mol. Biol.* **2015**, *17*, 1–10.
- [10] J. W. Pek, A. Anand, T. Kai, *Development* **2012**, *139*, 2255–2266.
- [11] R. Z. Jurkowska, S. Qin, G. Kungulovski, W. Tempel, Y. Liu, P. Bashtrykov, J. Stiefelmaier, T. P. Jurkowski, S. Kudithipudi, S. Weirich, R. Tamas, H. Wu, L. Dombrovski, P. Loppnau, R. Reinhardt, J. Min, A. Jeltsch, *Nat. Commun.* **2017**, *8*, 2057.
- [12] P. Mader, R. Mendoza-Sanchez, A. Iqbal, A. Dong, E. Dobrovetsky, V. B. Corless, S. K. Liew, S. R. Houliston, R. F. De Freitas, D. Smil, C. C. D. Sena, S. Kennedy, D. B. Diaz, H. Wu, L. Dombrovski, A. Allali-Hassani, J. Min, M. Schapira, M. Vedadi, P. J. Brown, V. Santhakumar, A. K. Yudin, C. H. Arrowsmith, *Bioorg. Med. Chem.* **2019**, *27*, 3866–3878.

Manuscript received: December 27, 2020

Accepted manuscript online: January 28, 2021

Version of record online: March 8, 2021